Dineutron structure in ^{8}He

Yoshiko Kanada-En'yo
Yukawa Institute for Theoretical Physics, Kyoto University, Kyoto, Japan
(Received 13 July 2007; published 29 October 2007)

The ground and excited states of ^{8}He were investigated with a method of antisymmetrized molecular dynamics (AMD). We adopted effective nuclear interactions that systematically reproduce the binding energies of ^{4}He, ^{6}He, and ^{8}He. The ground state of ^{8}He has both the j-j coupling feature ($p_{3/2}$ closure) and the L-S coupling feature ($^4\mathrm{He} + 2n + 2n$) with a slight tail of dineutron at the long distance region. The theoretical results give an indication of the 0_2^+ state with a dineutron gaslike structure, where two dineutrons are moving in an S wave around the α core with a dilute density. The dineutron structure ($^4\mathrm{He} + 2n + 2n$) of this state is similar to the 3α-cluster structure of the $^{12}\mathrm{C}(0_2^+)$ state, which has been interpreted as an α condensate state. Because the $^8\mathrm{He}(0_2^+)$ state has a significant overlap with the dineutron condensate wave function, we suggest that this theoretically predicted 0_2^+ state is a candidate for the dineutron condensate state.

DOI: 10.1103/PhysRevC.76.044323 PACS number(s): 21.60.−n, 02.70.Ns, 21.10.Ky

I. INTRODUCTION

In the recent study of unstable nuclear physics, various kinds of exotic structure have been discovered. Many of these phenomena in the light nuclear region are often related to cluster physics. For instance, the halo structure in ^{6}He and ^{11}Li and molecular structure in Be isotopes are regarded as cluster phenomena discovered in neutron-rich nuclei. Recently, Tohsaki *et al*. proposed a new type of cluster structure in the second 0^+ state ^{12}C, where 3α clusters are weakly interacting [1]. This is a dilute gas state of α particles that behave as bosonic particles in dilute density. This phenomena is associated with Bose-Einstein condensation and is called "alpha condensation." The alpha condensation was originally suggested in dilute nuclear matter by Röpke *et al*. [2]. The 0_2^+ of ^{12}C is regarded as an example where the alpha condensation is realized in a finite nuclear system. It is thus challenging to search for such cluster-gas states in other nuclei. In analogy to the alpha condensation, dineutron condensation in neutron matter is a recent key issue in the physics of unstable nuclei. Matsuo suggested that the dineutron correlation can be enhanced in dilute neutron matter [3]. In a real system, one should focus on the dineutron correlation in finite nuclei such as halo nuclei and extremely neutron rich nuclei or that in the neutron skin of neutron-rich nuclei. In fact, the dineutron correlation in two-neutron halo nuclei such as ^{6}He and ^{11}Li attracts great interests these days. For ^{6}He, where the ^{4}He is a good core, the dineutron correlation of valence neutrons has been demonstrated in three-body model calculations (see, e.g., Refs. [4–7] and references therein).

Now, let us consider the structure of ^{8}He from a point of view associated with the dineutron condensation. First, more than one dineutron is required to construct a dineutron condensate state. In ^{8}He, two pairs of neutrons can be formed around the ^{4}He core. Second, the ^{8}He system may have some correspondence with the ^{12}C system, because both systems have the same neutron number, $N = 6$. In analogy to ^{12}C, the ground state of ^{8}He may have a feature of the neutron $p_{3/2}$ closure or the SU(3)-limit p-shell configuration. Instead of the ground state, one can speculate a dineutron gas-like state with developed $^4\mathrm{He} + 2n + 2n$ structure in excited states.

There are many theoretical works on He isotopes. Application of *ab initio* calculations such as green function monte carlo (GFMC) and no-core shell model (NCSM) with realistic nuclear forces have reached the mass $A \sim 10$ region, including ^{6}He and ^{8}He [8–10]. Systematic studies of He isotopes have been performed also by model calculations with effective interactions such as cluster models as well as GSM [11–13] and mean-field approaches [14]. Three-body models with an assumption of the ^{4}He core have often been adopted to study ^{6}He [4–7,15,16] and they have been applied to heavier He isotopes [17]. ^{8}He and ^{10}He have been also studied by $^4\mathrm{He} + Xn$ models [18–21] and extended models [22,23]. With Fermionic molecular dynamics, the study of He isotopes has been performed based on a realistic nuclear force [24]. However, many of these studies concentrated on the ground states, except for the three-body models, GSM, and GFMC.

After the first experimental indication of neutron skin structure in ^{8}He [25], many experimental works of ^{8}He have been performed to reveal the detailed properties of the ground state. The core excitation $^6\mathrm{He}(2^+)$ in the ground state, which has been experimentally suggested [26], indicates that ^{8}He is different from a simple three-body state of $^6\mathrm{He}(0^+) + 2n$. Recent experiments using ^{8}He beams suggested a significant component of the $(p_{3/2})^2(p_{1/2})^2$ configuration [27,28]. They may support the dineutron correlation in the ^{8}He ground state rather than the pure $(p_{3/2})$ closure of neutrons. However, a measurement of the spectroscopic factor of $^7\mathrm{He}(3/2^-)$ [29] in ^{8}He suggested the pure subshell closed structure, contrasting with other experimental results. Thus, the neutron structure of the ^{8}He ground state is controversial. For excited states, some levels are known to exist in the energy $E_x = 3$–8 MeV region; however, the experimental information is very poor for these states except for the 2_1^+ state [30].

In this paper, we investigated the structure of ^{8}He. In particular, we focused on 0^+ states and discuss their dineutron component, because one of our major aims is to search for the dineutron gas-like state. We applied a method of antisymmetrized molecular dynamics (AMD) [31–33], which has been already proven to be useful in describing cluster structure in light nuclei. AMD has been applied to various light unstable

 ©2007 The American Physical Society

nuclei such as He, Li, and Be isotopes as well as stable nuclei. It has been applied also for the study of cluster gas-like states in ^{12}C and ^{11}C(^{11}B) [34,35]. In the present work, we adopted an AMD+generator coordinate method (GCM). Namely, we superposed a number of AMD wave functions, which were obtained by energy variation with constraints, to take various configurations into account. We comment that the theoretical method AMD+GCM of the present calculation is similar to those of the AMD+GCM and AMD+SSS works on He isotopes by Itagaki and his collaborators [20,23] in a sense that multiconfigurations of AMD wave functions are superposed. In Refs. [20,23], $^4\mathrm{He}+Xn$ and $t+t+Xn$ configurations were *a priori* assumed. Another claim is that they used an effective interaction that makes a bound ^2n. In the present work, we make no assumption on the cluster core and chose effective interactions by taking care of subsystem energies such as α-n and ^{6}He as well as nucleon-nucleon scattering. We used some sets of interaction parameters and showed the calculated results of the ground and excited states of He isotopes. By assuming a $(0s)^2$ configuration as the interior structure of a dineutron, we analyzed the dineutron structure of ^{8}He and compared it with the α-cluster structure of ^{12}C.

The paper is organized as follows. In the next section, we briefly explain the theoretical method of the present work. Results are given in Sec. III, and dineutron structure is discussed in Sec. IV. Finally, we give a summary in Sec. V.

II. FORMULATION

In this section, we briefly explain the formulation of AMD+GCM in the present calculation. The detailed formulation of the AMD method for nuclear structure study is described in Refs. [32,33]. There are various versions of practical methods of the AMD framework. In the present work, we performed a superposition of a number of AMD wave functions obtained by energy variation with constraints based on the concept of GCM. The procedure of the variation, spin and parity projection, and superposition is similar to those of AMD+GCM calculations in Refs. [20,36,37], though the details of the model wave functions and effective interactions are different from each other.

An AMD wave function is a Slater determinant of Gaussian wave packets,

$$\Phi_{\mathrm{AMD}}(\mathbf{Z}) = \frac{1}{\sqrt{A!}}\mathcal{A}\{\varphi_1, \varphi_2, \ldots, \varphi_A\}, \tag{1}$$

where the ith single-particle wave function is written by a product of spatial (ϕ), intrinsic spin (χ), and isospin (τ) wave functions as

$$\varphi_i = \phi_{\mathbf{X}_i}\chi_i\tau_i, \tag{2}$$

$$\phi_{\mathbf{X}_i}(\mathbf{r}_j) = \left(\frac{2\nu}{\pi}\right)^{\frac{3}{4}} \exp\left[-\nu\left(\mathbf{r}_j - \frac{\mathbf{X}_i}{\sqrt{\nu}}\right)^2\right], \tag{3}$$

$$\chi_i = \left(\frac{1}{2}+\xi_i\right)\chi_\uparrow + \left(\frac{1}{2}-\xi_i\right)\chi_\downarrow, \tag{4}$$

where $\phi_{\mathbf{X}_i}$ and χ_i are spatial and spin functions, and τ_i is the isospin function, which is fixed to be up (proton) or down (neutron). The width parameter ν is chosen to be the optimum value for each system. Accordingly, an AMD wave function is expressed by a set of variational parameters, $\mathbf{Z} \equiv \{\mathbf{X}_1, \mathbf{X}_2, \ldots, \mathbf{X}_A, \xi_1, \xi_2, \ldots, \xi_A\}$.

The energy variation was performed for the parity-projected AMD wave function $\Phi^{\pm}_{\mathrm{AMD}}(\mathbf{Z})$ under constraints. To obtain basis wave functions, we adopted the total oscillator quanta and deformation as the constraints. Hereafter, we note the expectation value of an operator $\hat{O}$ with respect to a normalized parity-projected AMD wave function as $\langle\hat{O}\rangle$. Expectation values $\langle\hat{N}^{\mathrm{ho}}\rangle$ of the total oscillator quanta are given by the creation and annihilation operators of the harmonic oscillator in the same way as in Ref. [37]. In the AMD+GCM calculations with the β-constraint (e.g., Ref. [36]), the deformation is usually constrained by using the rotational invariant value $D \equiv \mathrm{Tr}(QQ)/\mathrm{Tr}^2(Q)$, where the matrix Q is calculated by quadrupole operators as $Q_{\sigma\rho} = \langle\sum_i \hat{\sigma}_i\hat{\rho}_i\rangle$ ($\hat{\sigma} = \hat{x}, \hat{y}, \hat{z}$ and $\hat{\rho} = \hat{x}, \hat{y}, \hat{z}$) [38]. Here D is approximately related to the quadrupole deformation parameter β as $D(\beta) = (5\beta^2/2\pi + 1)/3$. In the present work, we used the modified quadrupole matrix $Q'_{\sigma\rho} \equiv Q_{\sigma\rho} - A\delta_{\sigma\rho}$ (where A is the mass number) instead of the original $Q_{\sigma\rho}$ and imposed the constraint on $D' \equiv \mathrm{Tr}(Q'Q')/\mathrm{Tr}^2(Q')$. This is useful for He isotopes to obtain basis wave functions with various configurations on mesh points of the two-dimensional parameters, β and $\langle\hat{N}^{\mathrm{ho}}\rangle$. The energy variation with the constraint values N_{const} and β_{const} was performed with respect to the parity-projected AMD wave function by minimizing the energy, defined as

$$E \equiv \langle\hat{H}\rangle + V^N(N_{\mathrm{const}} - \langle\hat{N}^{\mathrm{ho}}\rangle)^2 + V^\beta[D(\beta_{\mathrm{const}}) - D']^2. \tag{5}$$

Here the artificial potentials are introduced to satisfy the condition of the constraints. With a given set of constraint values $(N_{\mathrm{const}}, \beta_{\mathrm{const}})$ the optimum wave function $\Phi^{\pm}_{\mathrm{AMD}}(N_{\mathrm{const}}, \beta_{\mathrm{const}})$ was obtained. Finally, we superposed the spin-parity eigenstates projected from the obtained wave functions,

$$|^8\mathrm{He}(J^\pm_n)\rangle = \sum_{K, N_{\mathrm{const}}, \beta_{\mathrm{const}}} c^{J\pm}_n(K, N_{\mathrm{const}}, \beta_{\mathrm{const}}) \times |P^J_{MK}\Phi^{\pm}_{\mathrm{AMD}}(N_{\mathrm{const}}, \beta_{\mathrm{const}})\rangle, \tag{6}$$

where the coefficients $c^{J\pm}_n(K, N_{\mathrm{const}}, \beta_{\mathrm{const}})$ were determined by diagonalizing the Hamiltonian and Norm matrices. In the present calculations, we used all the $K = 0$ states. For the $K \neq 0$ states, we applied energy truncation and took only $P^J_{MK}\Phi^{\pm}_{\mathrm{AMD}}(N_{\mathrm{const}}, \beta_{\mathrm{const}})$ with energy $E \leqslant -10$ MeV.

III. RESULTS

A. Calculations

^{6}He, ^{8}He, and ^{10}He were calculated by the AMD+GCM method. The strengths, V^N and V^β, for the constraint potentials in Eq. (5) are chosen to be 30 and 2000 MeV, respectively. We chose the width parameter ν to optimize the energy for $P^{J=0}_{(MK)=(00)}\Phi^{+}_{\mathrm{AMD}}(N_{\mathrm{const}} = N_{\mathrm{min}} + 2)$, which gives the minimum energy among the states $P^{J=0}_{(MK)=(00)}\Phi^{+}_{\mathrm{AMD}}(N_{\mathrm{const}})$ in most cases. Here, N_{min} is the minimum value of the harmonic-oscillator quanta; $N_{\mathrm{min}} = 2$, 4, and 6 for ^{6}He, ^{8}He,

TABLE I. Parameter sets of the effective interaction and the values of the width parameter ν adopted in the present work. The theoretical values of scattering length $a_s(a_t)$ for singlet (triplet) even channel, neutron separation energy of ^{5}He[$S_n(^5\text{He}) \equiv E(^4\text{He}) - E(^4\text{He}\text{-}n)$], 2α threshold energy of ^{8}Be, and two-neutron separation energies of ^{6}He and ^{8}He[$S_{2n}(^6\text{He}) \equiv E(^4\text{He}) - E(^6\text{He})$ and $S_{2n}(^8\text{He}) \equiv E(^6\text{He}) - E(^8\text{He})$] are also listed.

Parameter set Central force		v58 Volkov No. 2	v56 Volkov No. 2	m62 MV1 case (3)	m56 MV1 case (3)
Wigner	w	0.42	0.44	0.38	0.44
Bartlett	b	0	0.15	0	0.15
Heisenberg	h	0	0.15	0	0.15
Majorana	m	0.58	0.56	0.62	0.56
$\nu(^4\text{He})$ (fm^{-2})		0.265	0.265	0.210	0.210
$\nu(^6\text{He})$ (fm^{-2})		0.245	0.245	0.210	0.210
$\nu(^8\text{He})$ (fm^{-2})		0.240	0.240	0.185	0.185
$\nu(^{10}\text{He})$ (fm^{-2})		0.185	0.175	0.165	0.165
	Exp.	v58	v56	m62	m56
a_t (fm)	5.42 (p-n)	9.7	5.4	6.4	4.2
a_s (fm)	−16.5 (n-n)	9.7	−23.9	6.4	>100
$S_n(^5\text{He})$ (MeV)	−0.9	−0.7	−0.7	−1.0	−0.4
$2E(^4\text{He}) - E(^4\text{He}\text{-}^4\text{He})$ (MeV)	−0.1	0.6	1.4	−1.3	−0.6
$S_{2n}(^6\text{He})$ (MeV)	1.0	1.3	−0.2	2.1	1.1
$S_{2n}(^8\text{He})$ (MeV)	2.1	3.0	3.2	1.2	2.0

and ^{10}He, respectively. A common ν value for each He isotope is used in the calculation with each interaction. The adopted ν values are listed in Table I. We adopted the constraint values of the mesh points (i, j) on the N_{const}-β_{const} plane as $N_{\text{const}}^{(i)} = N_{\min} + \Delta^{(i)}$($\Delta^{(i)} = 0, 1, 2, 3, 4, 6, 8, 10$ for positive-parity states and $\Delta^{(i)} = 1,2, 3, 4, 6, 8, 10$ for negative-parity states) and $\beta_{\text{const}}^{(j)} = 0, 0.2, 0.4, 0.6, \ldots, 1.6$. Then, the total number of the basis wave functions is 72 for positive-parity states and 63 for negative-parity states. On the N_{const}-β_{cont} plane, we first obtained the wave function $\Phi^{\pm}_{\text{AMD}}(N_{\text{const}}, \beta_{\text{const}})$ at $N_{\text{const}} = N_{\min} + 2$ and $\beta_{\text{const}} = 0, 0.2, 0.4, 0.6, \ldots, 1.6$. Then we searched for $\Phi^{\pm}_{\text{AMD}}(N_{\text{const}} + 1, \beta_{\text{const}})$ [or $\Phi^{\pm}_{\text{AMD}}(N_{\text{const}} - 1, \beta_{\text{const}})$] starting from the $\Phi^{\pm}_{\text{AMD}}(N_{\text{const}}, \beta_{\text{const}})$ by increasing (or decreasing) N_{const} one by one.

Some of the basis wave functions with these constraints contain breaking of the ^{4}He core. Such basis wave functions with ^{4}He-core breaking have high energies in general, and therefore, they give only a small contribution to the low-lying states of ^{6}He, ^{8}He, and ^{10}He isotopes. This means that the ^{4}He cluster is a rather good core in ^{6}He, ^{8}He, and ^{10}He isotopes, whereas the motion of valence neutrons is relatively important.

B. Interactions

We used an effective nuclear interaction consisting of the central force, the spin-orbit force, and the Coulomb force. For the central force, we adopted the Volkov force [39] used in the work on He isotopes with AMD+GCM ($^4\text{He} + Xn$) [20], and also the MV1 force [40] used in the AMD calculations of ^{12}C [34,42]. We used the spin-orbit force of the G3RS force [41] as done in Refs. [20,42]. We fixed the strengths of the spin-orbit term as $u_{ls} = 2000$ MeV, which is the same value as in Ref. [20]. By taking care of energies of subsystems, we tuned the interaction parameters, w, b, h, and m, for Wigner, Bartlett, Heisenberg, and Majorana exchange terms in the the central force (Volkov or MV1), respectively. ^{6}He, ^{8}He, and ^{10}He were calculated with AMD+GCM by using four cases of central force. The parametrization for the central force is summarized in Table I. To demonstrate characteristics of the effective interactions, we also show the relative energies of subsystems and the nucleon-nucleon scattering lengths with these four types of interaction. We estimate the energy of the ^{4}He, ^{4}He-n state with $J^\pi = 3/2^-$, and that of the ^{4}He-^{4}He state with $J^\pi = 0^+$, by assuming the $(0s)^4$ state of ^{4}He and performing cluster-GCM calculations within the α-n and α-α cluster models for simplicity.

The first case of interaction is the Volkov No. 2 force [39] with interaction parameters $m = 0.58$, $b = h = 0$. This is the same effective interaction as that used in the AMD+GCM ($^4\text{He} + Xn$) by Itagaki and Aoyama [20], which succeeded in systematically reproducing the binding energies of He isotopes. We denote this interaction as v58 in this paper. In spite of good agreement of the binding energies of He isotopes, the v58 force has a fault that two neutrons are bound in free space. It is well known that the Volkov force with $b = h = 0$ has a neutron-neutron attraction that is too strong, because such a parametrization with no Bartlett term nor Heisenberg term gives the same interaction in the singlet-even channel as that in the triplet-even channel. In reality, the singlet-even channel has weaker attraction, and two neutrons are unbound. To describe the dineutron correlation in neutron-rich nuclei it might be crucial to reproduce such a feature of a two-nucleon system, though it does not matter for a spin-isospin saturated system such as $Z = N$ nuclei.

In the second case of interaction, we used the Volkov No. 2 force with modified interaction parameters as $m = 0.56$, $b = h = 0.15$. This interaction (denoted v56) describes well the experimental S-wave scattering lengths of the n-n and p-n

channels and the unbound feature of two-neutron system. The Majorana parameter $m = 0.56$ was determined by adjusting the binding energy of ^{8}He to the experimental data. However, this interaction fails to reproduce $2n$ separation energies of ^{6}He and ^{8}He, and it also gives too strong an attraction in the ^{4}He-^{4}He system.

The third interaction (m62) and the fourth one (m56) listed in Table I are based on the MV1 force [40]. The parametrization of the m62 interaction is $m = 0.62$ and $b = h = 0$, which is the same as used in the AMD calculations of ^{12}C [34,42]. For the m62 interaction, two neutrons are bound infree space as well as the Volkov force with $b = h = 0$, like the v58 interaction. In the m56 interaction, we used the modified Bartlett and Heisenberg terms, $b = h = 0.15$, and the Majorana term $m = 0.56$, which was adjusted to reproduce the binding energy of ^{8}He. With the $m = 0.56$ interaction, two neutrons are almost unbound in free space, and the other subsystem energies are reasonably reproduced.

C. Ground states of He isotopes

We show the calculated results of the ground states of He isotopes. The energies of He isotopes are shown in Fig. 1. The v58 and m56 interactions systematically reproduce the energies of ^{4}He, ^{6}He, and ^{8}He, though they overestimate the ^{10}He energy. However, the v56 and m62 interactions are poor in reproducing the ^{6}He energy, and therefore, they fail to reproduce two-neutron separation energies of ^{6}He and ^{8}He as shown in Table I. Hereafter, we discuss the results obtained with the v58 and m56 interactions. We stress again that the v58 interaction well describes the subsystem energies except for the fault of the too strong neutron-neutron interaction, whereas the m56 interaction reasonably reproduces the global features of the subsystem energies.

The calculated root-mean-square radii of proton, neutron, and matter density are given in Table II. The experimental data and the theoretical results of other calculations are also listed. Experimentally, extremely large radii of ^{6}He and ^{8}He were reported by the reaction cross sections [25,43,44]. It was suggested that the large radii originate in the remarkable enhancement of neutron radii caused by the neutron halo and neutron skin structures in ^{6}He and ^{8}He, respectively. The empirical neutron radii are well described by the present calculations with the m56 interaction. However, the neutron radii calculated with the v58 interaction are slightly smaller than the empirical ones as well as the former AMD+GCM (^{4}He + Xn) calculations with the same v58 interaction [20]. The proton radii calculated with the m56 interaction are consistent with the observed data except for that of ^{4}He. Figure 2 shows the proton density and neutron density. In ^{6}He, the neutron density has a long tail at a large distance region. This is the neutron halo structure and is similar to the neutron density obtained by other calculations such as stochastic variational method (SVM) [19]. In ^{8}He, the neutron and proton density shows the neutron skin structure at the surface, which well corresponds to the discussion in Refs. [19,25]. Thus, the present calculations with the m56 interaction systematically describe the ground-state properties of ^{6}He and ^{8}He such as energies and radii.

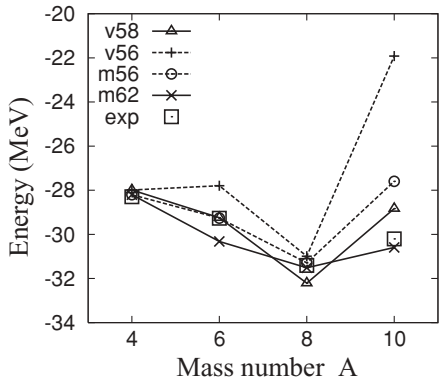

FIG. 1. The calculated energies of He isotopes with the v58, v56, m62, and m56 interactions (see text). The experimental data are also given.

TABLE II. Root-mean-square radii (fm) of point-proton, point-neutron, and point-matter density of the ground states of He isotopes. The experimental value (a) is deduced from the charge radius [46], and empirical values (b) are taken from Refs. [25,44]. Theoretical values of other calculations, NCSM [10], stochastic variational methods (SVM) [19], AMD+GCM (^{4}He + Xn) [20], and RMF [14], are also given.

		Exp.	AMD-v58	AMD-m56	SVM [19]	RMF [14]	AMD (^{4}He + Xn) [20]	NCSM [10]
^{4}He	r_p	1.455(1)	1.46	1.64				1.45
	r_n		1.46	1.64				1.45
	r_m		1.46	1.64		1.76		
^{6}He	r_p	1.912(18)[(a)]	1.83	1.90	1.80			1.89
	r_n	2.59–2.61[(b)]	2.40	2.49	2.67			2.67
	r_m	2.33–2.48[(b)]	2.23	2.31	2.46	2.43	2.32	
^{8}He	r_p	1.76–2.15[(b)]	1.76	1.96	1.71			1.88
	r_n	2.64–2.69[(b)]	2.37	2.63	2.53			2.8
	r_m	2.49–2.52[(b)]	2.24	2.48	2.40	2.55	2.31	
^{10}He	r_p		2.04	2.13				
	r_n		2.88	2.97				
	r_m		2.73	2.82		3.17		

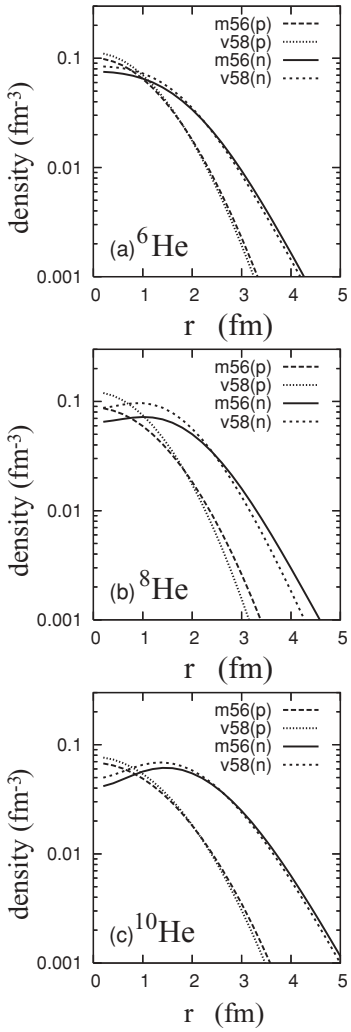

FIG. 2. Point-proton and point-neutron density in the ground states of He isotopes. The calculated results are those with the m56 and v58 interactions.

Let us discuss the effect of the spin-orbit force, which may induce the j-j coupling feature of neutrons. The expectation values of the spin-orbit force $\langle V_{ls}\rangle$ and those of the squared total intrinsic spin of neutrons $\langle S_n^2\rangle$ are listed in Table III. From the values of $\langle S_n^2\rangle$, the $S=1$ component in the ^{6}He(0_1^+) state is estimated to be 0.13 and 0.07 in the m56 and v58 results, respectively. This means that the $(p_{3/2})^2$ configuration is contained by the spin-orbit force. However, the $S=0$ component is still significant because of the L-S coupling feature of the spin-zero $2n$ correlation. We note that the fraction 0.87 in the m56 results for the $S=0$ component in ^{6}He is in good agreement with three-body model calculations [7,15,16,45]. Compared with the results of ^{6}He, where the L-S coupling configuration as well as the j-j coupling configuration is significant, the j-j coupling feature increases in the ^{8}He(0_1^+) state because of the $(p_{3/2})^4$ closure. As a result, the spin-orbit force gives a much larger attraction in ^{8}He (by a factor of 3–4) than in ^{6}He. It is interesting that the value $\langle S_n^2\rangle = 0.86$ (0.72) of the ^{8}He(0_1^+) in the m56 (v58) results is different from the value $\langle S_n^2\rangle = 1.33$ for the pure $(p_{3/2})^4$ closed state. This deviation is because the L-S coupling configuration is still present in ^{8}He owing to the spin-zero $2n$ correlation of neutron pairs. The detailed dineutron structure of ^{6}He and ^{8}He will be discussed later.

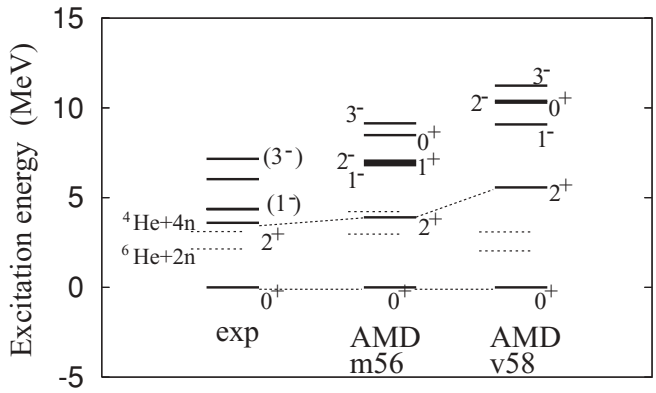

FIG. 3. Energy levels of ^{8}He. The calculated results are those with the m56 and v58 interactions. The experimental data are taken from Refs. [47] and [30].

D. Excited states of ^{8}He

The calculated energy levels of ^{8}He are illustrated in Fig. 3, and the properties of the excited states are shown in Table III. In both the m56 and v58 results, the 2_1^+ state is the lowest excited state and the 1_1^-, 2_1^-, 0_2^+, and 3_1^- states are obtained above the 2_1^+ state. In addition, in the present calculations with the m56 interaction, the 1_1^+ state is obtained at almost the same energy region as the 1_1^- and 2_1^- states. The present AMD framework is regarded as a kind of bound-state approximation because of the restricted model space, and therefore, coupling with continuum states is not taken into account. In such a case, only resonance states remain in the low-energy region; continuum states rise to a high excitation energy region in principle. Actually, below the calculated 3_1^- state, there are no other states than those presented in Fig. 3. However, to check the stability of these resonances against neutron decays, their properties should be carefully examined. In the present m56 results, the negative-parity states contain a large component of $^6\mathrm{He}+n+n$-like configurations with the valence neutron far from the core. Because they have extremely large neutron radii and show somehow escaping behavior of neutrons, further investigation is required for these negative-parity states. In particular, the 1_1^- and 2_1^- states can couple with the $(0s)^2(0p)^3(1s)^1$ neutron configuration, which has a valence $1s_{1/2}$ neutron with no centrifugal barrier.

Compared with the experimental data, the theoretical value of the 2_1^+ excitation energy is in good agreement with the experimental data in the m56 calculation, and it is slightly higher than the experimental one in the v58 case. However, it is important that the level structure for the excited states, 2_1^+, 1_1^-, 0_2^+, 2_1^-, and 3_1^-, is not sensitive to the adopted interaction though the relative position to the ground energy depends on the interaction. The 0_2^+ state is theoretically suggested to appear in the same energy region as the 1_1^-, 2_1^-, and 3_1^- states. What is striking is that the 0_2^+ state has a remarkably

TABLE III. Excitation energies, root-mean-square radii of point-proton, point-neutron, and point-matter density, the expectation values of squared total intrinsic spin of neutrons $\langle S_n^2 \rangle$, and those of the spin-orbit force $\langle V_{ls} \rangle$. The experimental data of the excitation energies are taken from Ref. [47].

		Exp.	AMD-v58						AMD-m56					
Nucleus	J_n^π	E_x (MeV)	E_x (MeV)	r_p (fm)	r_n (fm)	r_m (fm)	$\langle S_n^2 \rangle$	$\langle V_{ls} \rangle$ (MeV)	E_x (MeV)	r_p (fm)	r_n (fm)	r_m (fm)	$\langle S_n^2 \rangle$	$\langle V_{ls} \rangle$ (MeV)
^{6}He	2_1^+	1.797	2.5	1.80	2.41	2.22	0.24	−2.9	1.4	1.88	2.52	2.32	0.47	−2.8
^{6}He	0_1^+	0	0.0	1.83	2.40	2.23	0.16	−2.6	0.0	1.90	2.49	2.31	0.26	−2.3
^{8}He	3_1^-	7.16[a]	11.2	1.86	2.83	2.62	0.72	−7.6	9.1	2.06	3.25	3.00	1.15	−5.6
^{8}He	0_2^+		10.3	1.97	2.94	2.73	0.67	−4.7	8.5	2.11	3.12	2.90	0.99	−1.0
^{8}He	2_1^-		10.4	1.81	2.82	2.60	1.69	−11.0	7.1	2.07	3.32	3.06	1.92	−6.2
^{8}He	1_1^-	4.36[a]	9.1	1.85	2.85	2.63	0.88	−9.1	6.9	2.06	3.31	3.05	1.07	−6.0
^{8}He	1_1^+								6.8	1.97	2.86	2.67	2.02	−2.8
^{8}He	2_1^+	3.6[b]	5.6	1.80	2.55	2.38	0.25	−4.1	3.9	1.99	2.78	2.61	0.34	−2.7
^{8}He	0_1^+	0	0.0	1.76	2.37	2.24	0.72	−11.4	0.0	1.96	2.63	2.48	0.86	−7.3
^{10}He	0_1^+	0	0.0	2.04	2.88	2.73	0.13	−2.6	0.0	2.13	2.97	2.82	0.11	−1.7

[a]The spin and parity assignments for the 1^- and 3^- states have not been established yet.
[b]The excitation energy of the 2^+ is from Ref. [30].

large neutron radius compared with the ground state because of developed $^4\mathrm{He} + 2n + 2n$ structure. In the obtained wave function of the 0_2^+ state, which is given by a superposition of the basis AMD wave functions, the amplitude is found to be widely distributed into the basis wave functions with various spatial configurations of $^4\mathrm{He} + 2n + 2n$. This indicates a gas-like feature that the dineutrons are rather freely moving around the ^{4}He core. Therefore, we consider that the 0_2^+ state is a candidate for the cluster gas-like state with two dineutrons around the α core. The detailed discussion of the dineutron-like structure is given later. In the experimental energy spectra, some excited states were observed above the 2_1^+ state. Spins and parities of these states are not definitely assigned yet. In the present calculations, the predicted 0_2^+ state has a strong monopole neutron transition from the ground states as the matrix element $M_n(0_1^+ \to 0_2^+) = 13.5(13.9)\ \mathrm{fm}^2$ in the m56(v58) results. This neutron matrix element is much larger than the observed proton matrix element $M_p(0_1^+ \to 0_2^+) = 5.4\ \mathrm{fm}^2$ of ^{12}C by more than a factor of 2. Therefore, we consider that the $^8\mathrm{He}(0_2^+)$ might be excited by inelastic scattering on the nuclear target.

The excited states of ^{8}He have been theoretically predicted by a few other calculations such as continuum shell model (CSM) and GFMC. The CSM gives good agreement of the 2_1^+ excitation energy with the experimental data [12]. We also comment that the GFMC calculation with AV18/IL2, which is an *ab initio* calculation with a realistic two-body force and an empirical three-body force, gives a similar level structure of the positive-parity states to the present m56 results. Namely, the GFMC with AV18/IL2 gives the 2^+ state at $E_x = 4.72$ MeV and the 1_1^+, 0_2^+, and 2_2^+ states in the $E_x > 5$ MeV region.

IV. DINEUTRON STRUCTURE

A. What is a dineutron (^2n) cluster?

There is no bound state in an isolated *nn* system. However, it has been emphasized in many theoretical works that the spatial neutron-neutron correlation plays an important role in the binding mechanism of the Borromean systems with a two-neutron halo such as ^{6}He and ^{11}Li (e.g., Refs. [4–6,48] and references therein). The neutron-neutron correlation is characterized by a spin-zero *nn* pair with a spatial correlation in the *S* wave. In the correlation density of the two-neutron halo nuclei, a peak in the probability appears at the region with a small *n*-*n* distance [$R(nn)$] and a large *n*-core distance in general. This corresponds to the dineutron correlation. In an extended meaning, it is regarded as a "dineutron cluster," which can virtually exist in loosely bound neutron-rich nuclei.

As already mentioned, the characteristics of the dineutron are its zero spin and the spatial correlation. In the correlation density for ^{6}He, ^{11}Li, and ^{14}Be given by three-body calculations [5,7,49,50], the peak for the dineutron correlation is seen typically around $R(nn) \sim 2$ fm with a ridge in the $R(nn) = 2$–3 fm region. It is important that this *n*-*n* distance at the peak nearly depends on the system size among these three systems, ^{6}He, ^{11}Li, and ^{14}Be. From this most probable *n*-*n* distance, the typical size of the spatial correlation of the *nn* pair can be estimated to be about 2 fm. Then, to investigate the dineutron structure in ^{8}He, we here approximately describe the dineutron cluster, ^2n, by a spin-zero neutron pair written by the simple harmonic oscillator $(0s)^2$ state with the size parameter b. Then, the ^2n-cluster wave function $\phi^{^2n}(\mathbf{S})$, which is localized at the position $\mathbf{S}$, is expressed as

$$\phi^{^2n}(\mathbf{S}) = \mathcal{A}\left\{\phi_{\mathbf{S}}^{0s}(\mathbf{r}_1)\chi_\uparrow \phi_{\mathbf{S}}^{0s}(\mathbf{r}_2)\chi_\downarrow\right\}, \tag{7}$$

$$\phi_{\mathbf{S}}^{0s}(\mathbf{r}_i) = \frac{1}{(b^2\pi)^{\frac{3}{4}}} \exp\left[-\frac{1}{2b^2}(\mathbf{r}_i - \mathbf{S})^2\right]. \tag{8}$$

In this definition, the relative motion between two neutrons in the ^2n cluster is given by a Gaussian,

$$\phi^r(\mathbf{r}_1 - \mathbf{r}_2) = \frac{1}{(b_r^2\pi)^{\frac{3}{4}}} \exp\left[-\frac{1}{2b_r^2}(\mathbf{r}_1 - \mathbf{r}_2)^2\right], \tag{9}$$

with size $b_r = \sqrt{2}b$, which should be the typical *nn* distance $b_r = 2$–3 fm. With this approximation of the ^2n cluster, the

major component of the dineutron correlation might be taken into account, though the tail part at large correlation length is omitted. For simplicity, we chose the size parameter b for the $(0s)^2$ dineutron cluster as $b = 1/\sqrt{2\nu}$, where ν is the width parameter, $\nu(^6\text{He})$ and $\nu(^8\text{He})$ optimized for ^{6}He and ^{8}He, respectively, in the AMD calculations. The values of ν, which are listed in Table I, correspond to $b_r = 2.0$–2.3 fm and satisfy the typical nn distance of the dineutron correlation.

B. Dineutron-cluster motion

To investigate features of the dineutron cluster structure in the 0^+ states, we extracted the ^2n-cluster motion from the obtained $^8\text{He}(0^+)$ wave functions. We assume a simple core $(^4\text{He} + {}^2n)_{0^+}$, which is equivalent to the SU(3)-limit $^6\text{He}(0^+)$, and form the $^6\text{He}^{\text{SU(3)}}(0^+)$-$^2n$ cluster wave function with the $L = 0$ relative motion between the core $^6\text{He}^{\text{SU(3)}}(0^+)$ and the ^2n cluster. In the same way as in Refs. [34,51] for α-cluster motion, we calculated the reduced width amplitudes $ry(r)$ for the ^2n-cluster motion and the cluster probability S^{fac} by taking the overlap of the $^6\text{He}^{\text{SU(3)}}(0^+)$-$^2n$ cluster wave functions with the ^{8}He wave functions. In Fig. 4, we show the reduced width amplitudes in the $^8\text{He}(0_1^+)$ and the $^8\text{He}(0_2^+)$ wave functions obtained with the v58 and m56 interactions. These indicate the $^6\text{He}^{\text{SU(3)}}(0^+)$-$^2n$ relative motion. We also show the reduced width amplitudes for the $^8\text{Be}^{\text{SU(3)}}(0^+)$-$\alpha$ relative motion in $^{12}\text{C}(0_1^+)$ and $^{12}\text{C}(0_2^+)$ given in Ref. [42]. Surprisingly, the ^2n-cluster motion in ^{8}He is quite similar to the α-cluster motion in ^{12}C.

First we discuss the features of the dineutron clustering in the 0_2^+ state. The most striking thing is that the $^8\text{He}(0_2^+)$ state has a large amplitude of the dineutron cluster in the long distance region around $r = 4$–6 fm, which corresponds well to the peak position of the α-cluster motion in $^{12}\text{C}(0_2^+)$. The enhancement of the ^2n-cluster component at long distance is more remarkable in the v58 results than the m56 results. The cluster probability of $^8\text{He}(0_2^+)$, which is defined by the integrated overlap with the $^6\text{He}^{\text{SU(3)}}(0^+)$-$^2n$ cluster wave functions, is $S^{\text{fac}} = 0.50$ and $S^{\text{fac}} = 0.43$ in the v58 and the m56 results, respectively. The larger development of the ^2n clustering in the v58 results is considered to be because of the stronger n-n interaction in the v58 than in the m56 interaction. It is very important that, even with the weaker n-n interactions of the m56, the ^2n-cluster structure remains a significant component in $^8\text{He}(0_2^+)$. Considering that the other ^2n cluster exists inside the $^6\text{He}^{\text{SU(3)}}(0^+)$ core, it is regarded that $^8\text{He}(0_2^+)$ has a component of the developed $^4\text{He} + {}^2n + {}^2n$ clustering, where two dineutrons are moving in $L = 0$ orbits. Furthermore, from the analogy of the ^2n-cluster structure in $^8\text{He}(0_2^+)$ with the α-cluster structure in ^{12}C, $^8\text{He}(0_2^+)$ is considered to contain a dineutron gas-like structure.

Next, we discuss the dineutron structure in the ground state of ^{8}He. In $^8\text{He}(0_1^+)$, the reduced width amplitude has a peak at the distance of less than 3 fm. This means that the spatial development of the ^2n cluster is not so remarkable as that of $^8\text{He}(0_2^+)$. After discussing the dineutron structure in $^6\text{He}(0_1^+)$, we shall compare it with that of $^8\text{He}(0_1^+)$. In Fig. 4, we show the reduced width amplitudes of the ^{4}He-^2n cluster motion

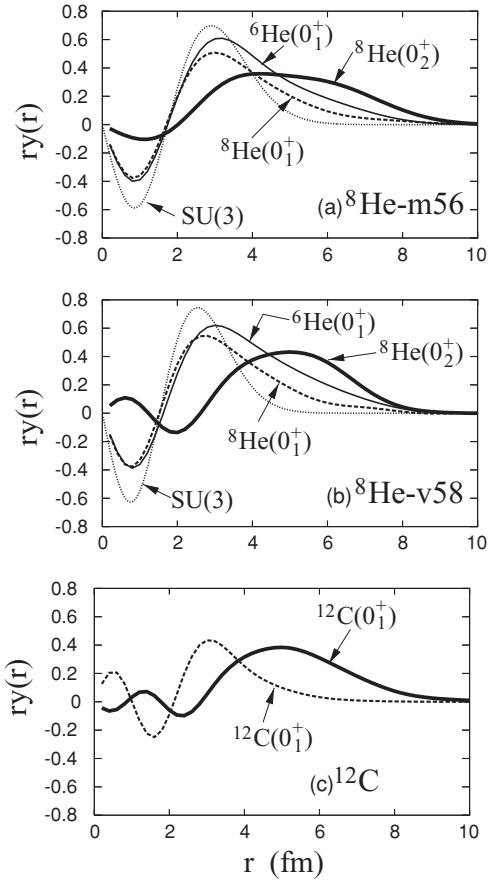

FIG. 4. Reduced width amplitudes $ry_{l=0}(r)$ for $^6\text{He}^{\text{SU(3)}}(0^+)$-$^2n$ in the $^8\text{He}(0^+)$, and those for ^{4}He-^2n in the $^6\text{He}(0^+)$. The $^8\text{He}(0^+)$ and $^6\text{He}(0^+)$ wave functions are calculated by AMD+GCM with (a) the v58 and (b) the m56 interactions. The $^6\text{He}^{\text{SU(3)}}(0^+)$ is written by an SU(3)-limit ^{4}He-$2n$ cluster state. The ^{4}He cluster and the ^2n cluster are expressed by the $(0s)^4$ and $(0s)^2$ wave functions, respectively, where the size parameter for the $(0s)$ state is chosen to be the same value as the AMD+GCM wave functions; $b = 1/\sqrt{2\nu(^6\text{He})}$ in the calculation of $ry(r)$ for $^6\text{He}(0^+)$ and $b = 1/\sqrt{2\nu(^8\text{He})}$ in the calculation of $ry(r)$ for $^8\text{He}(0^+)$. The reduced width amplitudes for ^{4}He-^2n in the $^6\text{He}^{\text{SU(3)}}(0^+)$ are also shown. (c) The reduced width amplitudes for $^8\text{Be}^{\text{SU(3)}}(0^+)$-$\alpha$ in the $^{12}\text{C}(0^+)$ taken from Ref. [34].

in $^6\text{He}(0_1^+)$ obtained by the present calculations and that in $^6\text{He}^{\text{SU(3)}}(0^+)$ given by the SU(3)-limit ^{4}He-^2n state. Compared with the SU(3)-limit, the calculated $^6\text{He}(0_1^+)$ wave function has a long tail of dineutron structure at the surface. The ^2n-cluster probability in the $^6\text{He}(0_1^+)$ state is $S^{\text{fac}} = 0.91$ and 0.84 in the v58 and the m56 calculations, respectively. This is consistent with the fractions, 0.92 and 0.87, of the $S = 0$ component, which are estimated from $\langle S_n^2 \rangle$. The ^2n-cluster probability is reduced by the $S = 1$ component because of the mixing of the $(p_{3/2})^2$ state. The dineutron wave function in the inner region is similar to that of the SU(3)-limit ^{4}He-^2n state. In this region, we have better to call it the spin-zero $2n$ correlation (dineutron correlation) rather than the ^2n cluster, because the antisymmetrization effect is important in the small distance region.

Comparing the result of ^{8}He(0^+_1) with that of ^{6}He(0^+_1), we found that the reduced width amplitude for the dineutron component is suppressed in ^{8}He(0^+_1). This is because of the $p_{3/2}$ subshell closure effect. As mentioned in the previous section, the j-j coupling feature is more remarkable in ^{8}He(0^+_1) than in ^{6}He(0^+_1). However, the cluster probability of ^{8}He(0^+_1) is still significant as $S^{\rm fac} = 0.57$ and 0.52 in the v58 and the m56 results, respectively. This probability dominantly originates in the SU(3)-limit $^4\mathrm{He} + {}^2n + {}^2n$ configuration, which is equivalent to the L-S coupling p-shell configuration, and indicates that the dineutron correlation is still important in ^{8}He(0^+_1). This situation is quite similar to that of ^{12}C(0^+_1), which is an admixture of the $p_{3/2}$ closure and the SU(3)-limit 3α state. As a result of the L-S coupling feature from the dineutron correlation, the ^{8}He(0^+_1) state should contain significant $(p_{3/2})^2(p_{1/2})^2$ contamination. This result is consistent with the experimental indication of the $p_{1/2}$ component in the ^{8}He ground state reported in recent observations [27,28]. As seen in Fig. 4, it is also interesting that the ^{8}He(0^+_1) state has a tail of the ^2n-cluster motion at the surface, though the tail is slight compared with the long tail in the ^{6}He(0^+_1) state. In conclusion, the ^{8}He(0^+_1) state is an admixture of the $p_{3/2}$ closure and the L-S coupling p-shell configuration of neutrons with a small tail of dineutron clustering.

C. ^2n condensate wave function

In the previous section, we discussed the ^2n-cluster wave function by assuming the core $(^4\mathrm{He} + {}^2n)_{0^+}$, which is equivalent to the SU(3)-limit ^{6}He(0^+). In this description, one of the ^2n clusters is confined in the the core $(^4\mathrm{He} + {}^2n)_{0^+}$, and its relative wave function to the ^{4}He is given by the $1s$ orbit of the harmonic oscillator potential with the oscillator frequency $\omega = 8\nu/3$.

As shown in Fig. 4, in this SU(3) limit, the radial wave function of the ^2n cluster around ^{4}He remains in the inner region. In such a case, although the ^2n cluster is moving in the S wave, it receives considerable antisymmetrization effect from the ^{4}He core and this does not necessarily indicate a gas-like state. To see more directly the ^2n-cluster gas-like nature, where two ^2ns are moving in the S wave far from the the ^{4}He core, we assumed the ^2n condensate wave function in the $^4\mathrm{He} + {}^2n + {}^2n$ system and calculated the overlap with the obtained ^{8}He(0^+) wave functions.

We define the ^2n condensate wave function by naturally extending the α condensate wave function proposed by Tohsaki *et al.* [1] as follows:

$$\Psi_{\rm cond}(B) \equiv n_0 \int \prod_{i=1}^{k} \left\{ d^3\mathbf{S}_i \exp\left(-\frac{(\mathbf{S}_i - \mathbf{S}_C)^2}{B^2}\right)\right\} \times \Phi_{\rm Brink}(\mathbf{S}_C, \mathbf{S}_1, \mathbf{S}_2, \ldots, \mathbf{S}_k), \quad (10)$$

where n_0 is the normalization factor and $\Phi_{\rm Brink}(\mathbf{S}_C, \mathbf{S}_1, \mathbf{S}_2, \ldots, \mathbf{S}_k)$ is the Brink wave function for the $C + k(^2n)$-cluster system consisting of a core (C) and k dineutrons (^2n) as

$$\Phi_{\rm Brink}(\mathbf{S}_C, \mathbf{S}_1, \mathbf{S}_2, \ldots, \mathbf{S}_k), \equiv \mathcal{A}\{\phi^C(\mathbf{S}_C)\phi^{^2n}(\mathbf{S}_1)\phi^{^2n}(\mathbf{S}_2)\cdots\phi^{^2n}(\mathbf{S}_k)\}. \quad (11)$$

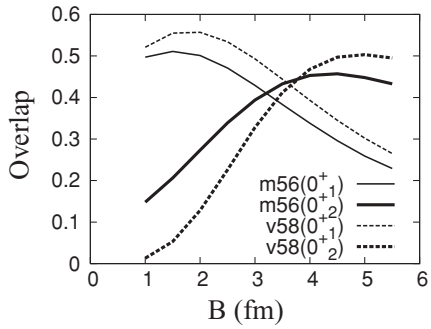

FIG. 5. The squared overlap between the dineutron condensate wave function $\Psi_{\rm cond}(B)$ and the obtained ^{8}He(0^+) wave functions. See details in the text.

Here, the wave function of the ith ^2n, $\phi^{^2n}(\mathbf{S}_i)$, is given by the $(0s)^2$ state localized around $\mathbf{S}_i$. $\mathbf{S}_C$ is the mean position of the center-of-mass motion of the core and is chosen to be $\mathbf{S}_C = -\frac{2}{A}(\mathbf{S}_1 + \mathbf{S}_2 + \cdots + \mathbf{S}_k)$. In the heavy limit of the core mass A, this wave function is equivalent to the dineutron condensate wave function proposed by Horiuchi [52]. In the present calculation for $^4\mathrm{He} + {}^2n + {}^2n$, the core C is ^{4}He, and the number of ^2n clusters is $k = 2$. We assumed the $(0s)^4$ state of the core wave function, $\phi^{^4\mathrm{He}}$, and adopted the common size parameter $b = 1/\sqrt{2\nu(^8\mathrm{He})}$ for the ^{4}He and ^2n clusters. In practical calculations, the six-dimensional integrals for the coordinates, $\mathbf{S}_1$ and $\mathbf{S}_2$, are performed by taking mesh points on $(\theta_{12}, |\mathbf{S}_1|, |\mathbf{S}_2|)$ and the total-angular-momentum projection (where θ_{12} is the angle between $\mathbf{S}_1$ and $\mathbf{S}_2$).

In Fig. 5, we show the squared overlap, $|\langle ^8\mathrm{He}|\Psi_{\rm cond}(B)\rangle|^2$, between the ^2n condensate wave function and the ^{8}He wave functions obtained by AMD+GCM. The calculated values are plotted as a function B, which indicates the size of the spatial distribution of the ^2n clusters in the condensate wave function. The ^{8}He(0^+_1) state has about 0.5 overlap at $B <$ 2 fm. The condensate wave function $\Psi_{\rm cond}(B)$ with such a small B is almost equivalent to the SU(3)-limit $^4\mathrm{He} + 2n + 2n$ state. In contrast, the ^{8}He(0^+_2) state has a maximum overlap, of about 0.5, at remarkably large size $B = 4$–5 fm. This is a strong indication of the dineutron gas-like component in the calculated ^{8}He(0^+_2). The dineutron gas-like feature is further enhanced in the v58 interaction than in the m56 interaction. These results are consistent with the discussion of the ^2n-cluster wave function in the previous section.

V. SUMMARY

We studied the structure of ^{8}He with the AMD+GCM method. We chose the effective nuclear interactions by taking care of energies of subsystems and reproduced the ground-state properties of ^{4}He, ^{6}He, and ^{8}He. In the ground state of ^{8}He, the $p_{3/2}$ subshell closure is a dominant component. However, the L-S coupling feature is also significant because of the spin-zero dineutron correlation. This is consistent with the experimental report on the significant mixing of the $(p_{3/2})^2(p_{1/2})^2$ component in ^{8}He(0^+_1). It is concluded that the ^{8}He(0^+_1) state is an admixture of $p_{3/2}$ subshell

closure and L-S coupling p-shell configurations with a slight dineutron tail at the surface. This result is also consistent with the experimentally suggested large spectroscopic factor of ^{6}He(2^+) in ^{8}He(0_1^+).

The present results suggest that the 0_2^+ state may appear near the negative-parity states above the 2_1^+ state. By analyzing dineutron structure, it was found that this state has a significant component of the developed $^4\mathrm{He} + {}^2n + {}^2n$ structure where two dineutrons are moving around the ^{4}He core in the S wave with a dilute density. The ^2n-cluster wave function of the ^{8}He(0_2^+) state is similar to the α-cluster wave function of the ^{12}C(0_2^+) state. Therefore, we consider that the predicted ^{8}He(0_2^+) state is a candidate for a dineutron gas-like state, which is analogous to the α condensate state suggested in ^{12}C(0_2^+). In the experimental energy spectra of ^{8}He, some excited states were observed above the 2_1^+ state. Spins and parities of these states have not been definitely assigned yet. Since the present calculations predicted the remarkable neutron matrix element for the monopole transitions $^8\mathrm{He}(0_1^+) \rightarrow {}^8\mathrm{He}(0_2^+)$, we expect that the ^{8}He(0_2^+) state might be excited in inelastic scattering on nuclear targets.

The AMD framework is regarded as a kind of bound-state approximation, so coupling with continuum states is not taken into account. Moreover, because of the restricted model space, particle-hole excitations may be only partially included but are not fully treated. In future, widths of the excited states should be carefully investigated with further large basis calculations by taking into account the continuum coupling to confirm the stability of the resonances against particle decays.

In the present work, the calculations were performed within the AMD model space by using effective interactions. We chose the interaction parameters by taking care of subsystem energies such as those of α-n and ^{6}He, as well as the scattering lengths of nucleon-nucleon systems. Although it is difficult to completely reproduce all of the subsystem energies with a unique effective interaction, we found interaction parameter sets that can reasonably reproduce the global feature of the subsystem energies. We here stress that the level structure of the excited states is not sensitive to the adopted nuclear forces within the reasonable choice of effective interaction, though the excitation energy relative to the ground state depends on the interaction. It is also important that the dineutron structure of the ^{8}He(0^+) states is qualitatively similar among the four sets of interaction adopted in the present calculations. For further investigations of He isotopes, more extended calculations based on realistic forces should be important as well as *ab initio* calculations.

ACKNOWLEDGMENTS

The authors would like to thank Prof. Horiuchi, Prof. Tohsaki, and their collaborators for valuable discussions. They are also thankful to members of the Yukawa Institute for Theoretical Physics (YITP) and the Department of Physics, Kyoto University, especially to Dr. Takashina for fruitful discussions. The computational calculations in this work were performed by the Supercomputer Projects of High Energy Accelerator Research Organization (KEK) and also the super computers of YITP. This work was supported by a Grant-in-Aid for Scientific Research from JSPS. It is also supported by the Grant-in-Aid for the 21st Century COE "Center for Diversity and Universality in Physics" from MEXT. Discussions in the RCNP workshops on cluster physics held in 2007 and those in the workshops YITP-W-06-17 and YITP-W-07-01 held at YITP were helpful to initiate and complete this work.

[1] A. Tohsaki, H. Horiuchi, P. Schuck, and G. Röpke, Phys. Rev. Lett. **87**, 192501 (2001).
[2] G. Röpke, A. Schnell, P. Schuck, and P. Nozieres, Phys. Rev. Lett. **80**, 3177 (1998).
[3] M. Matsuo, Phys. Rev. C **73**, 044309 (2006).
[4] G. F. Bertsch and H. Esbensen, Ann. Phys. (NY) **209**, 327 (1991).
[5] M. V. Zhukov *et al*., Phys. Rep. **231**, 151 (1993).
[6] S. Aoyama, K. Kato, and K. Ikeda, Prog. Theor. Phys. Suppl. **142**, 35 (2001).
[7] K. Arai, Y. Ogawa, Y. Suzuki, and K. Varga, Prog. Theor. Phys. Suppl. **142**, 97 (2001).
[8] S. C. Pieper, R. B. Wiringa, and J. Carlson, Phys. Rev. C **70**, 054325 (2004).
[9] S. C. Pieper, Nucl. Phys. **A751**, 516c (2005).
[10] E. Caurier and P. Navrátil, Phys. Rev. C **73**, 021302(R) (2006).
[11] N. Michel, W. Nazarewicz, M. Ploszajczak, and J. Okolowicz, Phys. Rev. C **67**, 054311 (2003).
[12] A. Volya and V. Zelevinsky, Phys. Rev. Lett. **94**, 052501 (2005); Phys. Rev. C **74**, 064314 (2006).
[13] G. Hagen, M. Hjorth-Jensen, and J. S. Vaagen, Phys. Rev. C **71**, 044314 (2005).
[14] Y. Sugahara *et al*., Prog. Theor. Phys. **96**, 1165 (1996).
[15] A. Csótó, Phys. Rev. C **48**, 165 (1993).
[16] D. Baye, M. Kruglanski, and M. Vincke, Nucl. Phys. **A573**, 431 (1994).
[17] S. Aoyama, Phys. Rev. Lett. **89**, 052501 (2002).
[18] Y. Suzuki and W. J. Ju, Phys. Rev. C **41**, 736 (1990).
[19] K. Varga, Y. Suzuki, and Y. Ohbayasi, Phys. Rev. C **50**, 189 (1994).
[20] N. Itagaki and S. Aoyama, Phys. Rev. C **61**, 024303 (1999).
[21] H. Masui, K. Katō, and K. Ikeda, Phys. Rev. C **75**, 034316 (2007).
[22] A. Doté and H. Horiuchi, Prog. Theor. Phys. **103**, 261 (2000).
[23] S. Aoyama, N. Itagaki, and M. Oi, Phys. Rev. C **74**, 017307 (2006).
[24] T. Neff, H. Feldmeier, and R. Roth, Nucl. Phys. **A752**, 321c (2005).
[25] I. Tanihata *et al*., Phys. Lett. **289B**, 261 (1992).
[26] A. A. Korsheninnikov *et al*., Phys. Rev. Lett. **90**, 082501 (2003).
[27] L. V. Chulkov *et al*., Nucl. Phys. **A759**, 43 (2005).
[28] N. Keeley *et al*., Phys. Lett. **B646**, 222 (2007).
[29] F. Skaza *et al*., Phys. Rev. C **73**, 044301 (2006).
[30] A. A. Korsheninnikov *et al*., Phys. Lett. **B316**, 38 (1993).
[31] Y. Kanada-En'yo, H. Horiuchi, and A. Ono, Phys. Rev. C **52**, 628 (1995); Y. Kanada-En'yo and H. Horiuchi, *ibid.* **52**, 647 (1995).
[32] Y. Kanada-En'yo and H. Horiuchi, Prog. Theor. Phys. Suppl. **142**, 205 (2001).
[33] Y. Kanada-En'yo, M. Kimura, and H. Horiuchi, C. R. Phys. **4**, 497 (2003).

[34] Y. Kanada-En'yo, Prog. Theor. Phys. **117**, 655 (2007).
[35] Y. Kanada-En'yo, Phys. Rev. C **75**, 024302 (2007).
[36] M. Kimura and H. Horiuchi, Prog. Theor. Phys. **111**, 841 (2004).
[37] Y. Kanada-En'yo and Y. Akaishi, Phys. Rev. C **69**, 034306 (2004).
[38] A. Dote, H. Horiuchi, and Y. Kanada-En'yo, Phys. Rev. C **56**, 1844 (1997).
[39] A. B. Volkov, Nucl. Phys. **74**, 33 (1965).
[40] T. Ando, K. Ikeda, and A. Tohsaki, Prog. Theor. Phys. **64**, 1608 (1980).
[41] N. Yamaguchi, T. Kasahara, S. Nagata, and Y. Akaishi, Prog. Theor. Phys. **62**, 1018 (1979); R. Tamagaki, *ibid*. **39**, 91 (1968).
[42] Y. Kanada-En'yo, Phys. Rev. Lett. **81**, 5291 (1998).
[43] I. Tanihata *et al*., Phys. Rev. Lett. **55**, 2676 (1985).
[44] I. Tanihata *et al*., Phys. Lett. **B206**, 592 (1988).
[45] K. Hagino and H. Sagawa, Phys. Rev. C **72**, 044321 (2005).
[46] L.-B. Wang *et al*., Phys. Rev. Lett. **93**, 142501 (2004).
[47] D. R. Tilley *et al*., Nucl. Phys. **A745**, 155 (2004).
[48] S. Aoyama, A. Muraki, K. Katō, and K. Ikeda, Prog. Theor. Phys. **93**, 99 (1995).
[49] P. Descouvemont, C. Daniel, and D. Baye, Phys. Rev. C **67**, 044309 (2003).
[50] P. Descouvemont, E. Tursunov, and D. Baye, Nucl. Phys. **A765**, 370 (2006).
[51] Y. Kanada-En'yo and H. Horiuchi, Phys. Rev. C **68**, 014319 (2003).
[52] H. Horiuchi, Mod. Phys. Lett. A **21**, 2455 (2006).